


Article

An Experimental Study of Fluoride Removal from Wastewater by Mn-Ti Modified Zeolite

Bo Yang¹, Guirong Sun¹, Bingxu Quan¹, Jiawei Tang², Chunhui Zhang^{1,*}, Chaomin Jia¹, Yuanhui Tang¹, Xinling Wang¹, Mengmeng Zhao¹, Wenqian Wang¹ and Binhu Xiao³

¹ School of Chemical and Environmental Engineering, China University of Mining and Technology (Beijing), Beijing 100083, China; BQT1800302029@student.cumtb.edu.cn (B.Y.); s1228230577@163.com (G.S.); quanbingxu@hotmail.com (B.Q.); SQT2000302066@student.cumtb.edu.cn (C.J.); tangyuanhui@126.com (Y.T.); 15030775113@163.com (X.W.); SQT2000302081@student.cumtb.edu.cn (M.Z.); 13994775648@163.com (W.W.)

² State Key Laboratory of Water Resource Protection and Utilization in Coal Mining, Beijing 102211, China; angpdh24tjw@hotmail.com

³ Produce and Technology Department, China Coal Shaanxi Yulin Energy and Chemical Co., Ltd., Yulin 719000, China; 15030531019@163.com

* Correspondence: ZHCumtb@hotmail.com; Tel.: +86-13910176209

Abstract: The emerging interest in fluoride-removal from wastewater has attracted attention to zeolite since it has been considered as a natural adsorbent. However, the fluoride-removal efficiency of natural zeolite is generally low. As part of the effort to improve the zeolite adsorption efficiency, we have produced and tested the Mn-Ti modified zeolite. In the current work, the material preparation is discussed, and prepared materials were characterized by X-ray diffraction (XRD), energy dispersive X-ray spectroscopy (EDS), scanning electron microscopy, and Fourier transform infrared (FTIR) spectra. Both static and dynamic experiments were conducted to examine the effects of independent variables. In the static adsorption section, sensitivity analysis experiments were conducted for independent variables, such as adsorbent dosage, pH, temperature, and competitive ions. The maximum adsorption capacity is 2.175 mg/g, which was obtained at PH = 7, temperature = 25 °C, and initial fluoride concentration = 10 mg/L. For adsorption kinetics, both Lagergren and Pseudo-second order models predict the experiments very well, which probably demonstrates that the current process is a combination of physical sorption and chemisorption. For adsorption isotherms, the Freundlich model performs better than the Langmuir model since it is usually applied to illustrate adsorption on inhomogeneous surfaces. In the dynamic adsorption section, sensitivity analysis experiments were also conducted for independent variables, such as adsorbent thickness, flow velocity, initial fluoride concentration, and PH. Additionally, the adsorption mechanism is also discussed. The main reason is the hydrated metal fluoride precipitate formation. As we know, the current work provides the first quantified comparison of the natural zeolite and the Mn-Ti modified zeolite regarding fluoride-removal efficiency.

Keywords: fluoride-removal; Mn-Ti modified zeolite; water treatment; adsorption mechanism



Citation: Yang, B.; Sun, G.; Quan, B.; Tang, J.; Zhang, C.; Jia, C.; Tang, Y.; Wang, X.; Zhao, M.; Wang, W.; et al. An Experimental Study of Fluoride Removal from Wastewater by Mn-Ti Modified Zeolite. *Water* **2021**, *13*, 3343. <https://doi.org/10.3390/w13233343>

Academic Editor: Layla Ben Ayed

Received: 20 October 2021

Accepted: 19 November 2021

Published: 25 November 2021

Publisher's Note: MDPI stays neutral with regard to jurisdictional claims in published maps and institutional affiliations.



Copyright: © 2021 by the authors. Licensee MDPI, Basel, Switzerland. This article is an open access article distributed under the terms and conditions of the Creative Commons Attribution (CC BY) license (<https://creativecommons.org/licenses/by/4.0/>).

1. Introduction

Fluoride is present in groundwaters, especially in regions containing fluoride-rich minerals. In the Guidelines for Water Quality [1] published by the WHO or World Health Organization, the upper limit of the fluoride concentration in edible water is advocated to be 1.5×10^{-3} g/L. As discussed in the literature [1], low-concentration fluoride is a favorable ingredient for human beings respecting the dental health. The positive impacts of fluoride increment with its concentration up to about 2×10^{-3} g/L. Notwithstanding its positive effects on dental health, there is a growing evidence exhibiting that elevated fluoride intakes can incite severe tissue lesion on bones. For instance, skeletal fluorosis may develop when fluoride ion concentration in edible water is higher than 3×10^{-3} g/L, which has the potential to cause painful damage to bones and joints.

High-fluoride concentration groundwaters appeared in many regions, particularly in parts of China, India, South America, and Central Africa [1–5]. Subsequently, numerous people are facing the challenge of the daily exposure to high-fluoride concentration drinking water and associated health issues. For example, Handa reported that well waters of several locations in India contain fluoride as high as 20 ppm [2]. In order to inhibit the adverse impacts of high-fluoride concentration drinking water, many fluoride-removal strategies have been proposed, such as electrochemical coagulation [6], ion exchange [7], precipitation [8], electrodialysis [9–11], reverse osmosis [12–15], adsorption [16–21], and so on. Among these strategies, adsorption-based strategies have the scalability potentiality because of their cost-efficiency. For example, natural adsorbents, such as zeolites [16–18], are encouraging as a result of local-availability and cost-efficiency. Additionally, nano-adsorbents, such as titanium oxide [22–24] and manganese oxide [25,26], have also been considered as a developing pollutant-removal technique. Nanosized manganese oxide is not only an effective fluoride adsorbent [26,27], but also one of the most important scavengers of aqueous trace metals [28]. Nanosized titanium oxide, on the other hand, is also proposed to be a non-toxic and stable fluoride adsorbent [29]. It is nonetheless the case that the high recovery cost of nanoparticles is becoming a primary obstacle to their practical applications on a large scale [24]. Consequently, an emerging research direction is to reduce the cost by immobilizing nanoparticles on supports. Zeolite is a candidate of the supports in virtue of its distinguished adsorption capacity regarding its high surface areas from its naturally formed pores and channels [24,30]. Accordingly, aqueous pollutant-removal strategies based on Mn or Ti modified zeolites have been substantially investigated [24,28,31–36]. Liu et al. [24] studied rapid humic acid adsorption of titanium modified natural zeolite. Camacho et al. [33] studied arsenic removal by manganese oxide modified natural clinoptilolite zeolite. Zou et al. [34,35] studied copper (II) and lead (II) ion removal of manganese oxide modified zeolite. Lyu et al. [36] studied manganese removal of manganese oxide modified zeolite. These studies demonstrate the potential to adopt Mn or Ti modified zeolites on aqueous pollutant removal. There is, nonetheless, a lack of a study of fluoride-removal using a Mn-Ti modified zeolite and the joined effects of Mn and Ti oxides.

In the current study, the aqueous fluoride-removal by a Mn-Ti modified zeolite was assessed experimentally. Adsorbent preparation and characterization are first discussed in this paper. This is followed by experimental results, such as adsorption kinetics and isotherms, and a discussion about the adsorption mechanism. Finally, some conclusions are given. The major objective of the paper is to thoroughly describe the fluoride-removal capability of the Mn-Ti modified zeolite.

2. Material Preparation and Experimental Methodology

2.1. Preparation of the Mn-Ti Modified Zeolite

2.1.1. Nano-Manganese Oxide Synthesis

The chemicals used in this study, including potassium permanganate (KMnO_4), manganese sulfate ($\text{MnSO}_4 \cdot \text{H}_2\text{O}$), absolute ethanol ($\text{CH}_3\text{CH}_2\text{OH}$), tetrabutyl orthotitanate ($\text{C}_{16}\text{H}_{36}\text{O}_4\text{Ti}$), acetic acid ($\text{C}_2\text{H}_4\text{O}_2$), nitric acid (HNO_3), and potassium hydroxide (KOH), were obtained from Sinopharm Chemical Reagent CO., Ltd., and were all of analytical reagent (AR) grade unless other specified. The nanosized manganese oxide synthesis methodology has been extensively explored [37–39]. In the current study, nano-manganese oxide was manufactured in house. Firstly, potassium permanganate (KMnO_4) solution was obtained by dissolving 3.75 g KMnO_4 in 2×10^{-2} L purified water. In the same way, manganese sulfate (MnSO_4) solution was prepared by dissolving 0.67 g manganese sulfate monohydrate ($\text{MnSO}_4 \cdot \text{H}_2\text{O}$) in 8×10^{-2} L purified water. Secondly, the MnSO_4 solution was mixed with KMnO_4 solution by keeping the mole ratio of MnO_4^- and Mn^{2+} as 6 to 1. A magnetic rotor was applied to stir for 30 min at 1200 rpm until the solution is adequately mixed. The mixed blend was then sealed with a 0.15 L autoclave and placed into a dry box preheated to 140 °C for 12 h. Thirdly, after neutralization using 0.1 mol/L

potassium hydroxide (KOH), the heated blend was cooled down to room temperature. Finally, nanosized manganese oxide was obtained by collecting the precipitate in the blend (filtering off the blend; washing the precipitate using deionized water for 3–4 times; drying it at 80 °C; grinding it into powder). The obtained nanosized manganese oxide is used in the following section to prepare the Mn-Ti modified zeolite. The detailed process is shown in Figure 1.

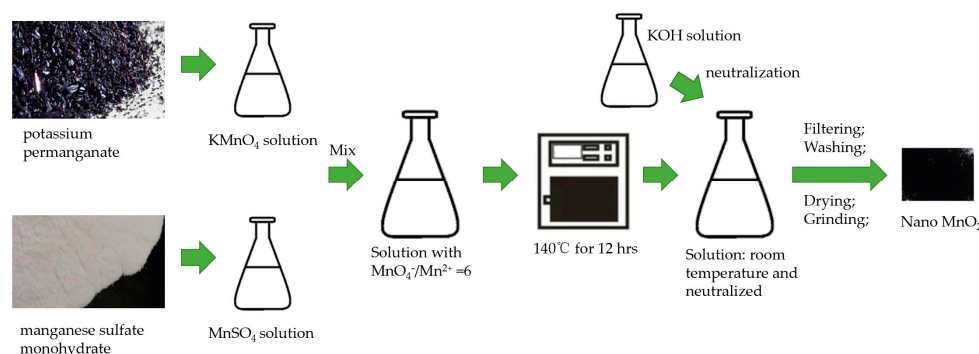


Figure 1. Schematic of Mn-Ti modified zeolite preparation.

2.1.2. Mn-Ti Modified Zeolite Preparation

The Mn-Ti modified zeolite preparation procedure consists of 6 steps. Firstly, a solution A was prepared by mixing 1×10^{-2} L Tetrabutyl orthotitanate ($C_{16}H_{36}O_4Ti$) and 3.5×10^{-2} L ethanol anhydrous (C_2H_5OH) at room temperature under magnetic stirring. At the same time, 4 mL Acetic acid ($C_2H_4O_2$) was slowly added as an inhibitor. A clear yellow solution A was obtained by using a magnetic rotor to stir at 1000 rpm for 40 min. Secondly, a solution B was prepared by mixing 0.1 mol/L nitric acid (HNO_3) to a blend of 1×10^{-2} L of water (H_2O) and 3.5×10^{-2} L of ethanol (C_2H_5OH) to achieve the target pH of the solution as $PH = 4$. Thirdly, a light-yellow solution C was obtained by dropping solution B into solution A at a constant rate, 3×10^{-3} L/min, under 1200 rpm magnetic stirring. Fourthly, a white gel D was obtained by adding 24 g of natural zeolite and 24 g of nanosized manganese dioxide powder to solution C in a ratio of 1:1, stirring for 1 h, and aging for 10 h. Fifthly, a modified zeolite powder was obtained by drying and grinding the white gel in an oven at 105 °C. Finally, the Mn-Ti modified zeolite was obtained by roasting the powder at 773 K in a muffle furnace for at least 2 h. The detailed process is shown in Figure 2.

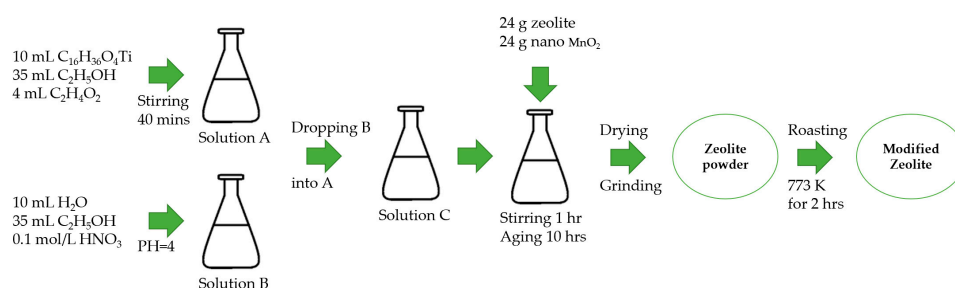


Figure 2. Mn-Ti modified zeolite preparation schematic.

2.2. Adsorbent Characterization

The XRD (D8-Advanced, Bruker Ltd., Bremen, Germany) patterns of the natural and the modified zeolites were achieved by taking advantage of Cu irradiation (10–80°). Photomicrography analyses of chemical and physical properties of the natural and the Mn-Ti modified zeolites were investigated by taking advantage of the typical material characterization facilities, such as EDS (Model EX-250, Horiba, Japan) and SEM (Model s-4800,

Hitachi, Japan). Additionally, a NICOLET iS10 spectrometer (Thermo Nicolet, USA) was applied to obtain the FTIR spectra. Similar procedures of the analyses can be found in [28,33]. Although not discussed extensively in the manuscript, zero point of charge (PZC) was also measured for the modified zeolite. For example, the mass titration method was applied for determination of the PZC, and it was found to be 5.1 ± 0.5 . This property identifies the surface charge of the adsorbent. Additionally, an N2 Adsorption test (ASAP2460, Micromeritics, Norcross, GA, USA) was conducted to measure the BET surface area of the modified zeolite, which was $6.3960 \text{ m}^2/\text{g}$. This value is much higher than the BET surface area of natural zeolite, $1.2530 \text{ m}^2/\text{g}$. The reason for the obvious increase in the specific surface area of the modified zeolite is the loading of surface nanomaterials, which provides more adsorption sites for fluoride.

2.3. Experimental Methodology

2.3.1. Static Experiments

To investigate the adsorption effectiveness of the Mn-Ti modified zeolite, independent variables, such as adsorbent dosage, pH, competitive ions, as well as adsorption kinetics and isotherms were studied in a static environment. For the study of adsorption dosage, adsorption time history was measured and analyzed for a solution with varying amounts, 0.1, 0.4, 0.8, 1, 1.5, 2, 2.5, and 3 g, of the Mn-Ti modified zeolite placed in $2.5 \times 10^{-2} \text{ L}$ wastewater with $1 \times 10^{-2} \text{ g/L}$ initial fluoride concentration. The same method was applied to study the pH effect over the pH range of 3 to 11 for a 0.1 L wastewater (synthetic wastewater: pure water containing fluoride) solution with 2 g Mn-Ti modified zeolite and $1 \times 10^{-2} \text{ g/L}$ initial fluoride concentration. For the study of competitive ions, 0.3 g/L competitive ion was added into the wastewater. The test time was set to 4 h and the test temperature was $25 \text{ }^\circ\text{C}$. After 4 h, the remaining fluoride concentration was measured, and the corresponding adsorption rate (or fluoride-removal rate) was calculated. The 4-h test time was selected to produce a sensitive test condition and to provide an efficient experimental procedure. Adsorption kinetics and isotherms were also studied. Typical adsorption kinetic mechanisms, such as Lagergren model and pseudo-second order model, and typical adsorption isotherm mechanisms, such as Langmuir model and Freundlich isotherm model, were compared with the experimental results and discussed.

2.3.2. Dynamic Experiments Using an Adsorption Column

To study the adsorption capability of the Mn-Ti modified zeolite in practical flow systems, a 1500 mm long and 20 mm-diameter adsorption column was designed to measure fluoride-removal rate in a dynamic system. The fluoride-containing wastewater (synthetic wastewater: pure water containing fluoride) flowed through the adsorption column. The baseline setting was $1 \times 10^{-2} \text{ g/L}$ initial fluoride concentration, $\text{pH} = 7$ and flow speed = 4 mL/min. Effects of adsorbent thickness, flow velocity, and initial fluoride concentration were studied by adjusting the independent variables. Adsorbent thickness was tested at 40 cm, 60 cm and 80 cm; flow velocity was tested at 4 mL/min, 6 mL/min and 8 mL/min; initial fluoride concentration was tested at $3 \times 10^{-3} \text{ g/L}$, $5 \times 10^{-3} \text{ g/L}$ and $1 \times 10^{-2} \text{ g/L}$; pH was tested at $\text{PH} = 4$, $\text{PH} = 7$, and $\text{PH} = 10$.

3. Results and Discussion

3.1. Material Characterization and Crystallinity

3.1.1. The Natural Zeolite Composition

Powder diffraction pattern of the natural zeolite is shown in Figure 3. XRD measurement was conducted to obtain the major crystalline phases in the natural zeolite. The reference patterns of typical zeolites [40] were compared with the measured results. Gismondine was found to be the main component of the natural zeolite discovered in Henan, China.

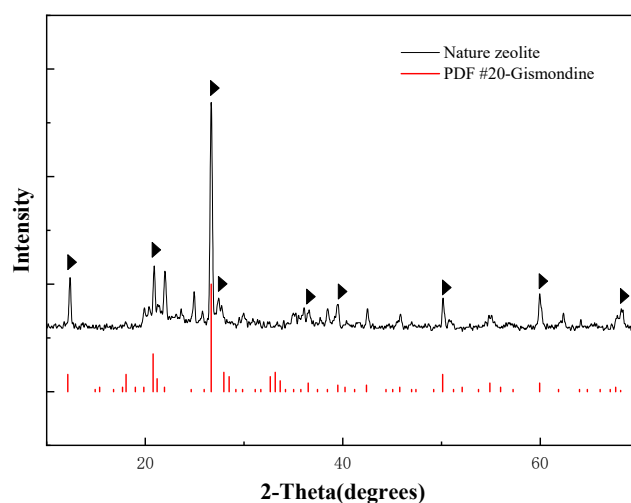


Figure 3. XRD measurement of the unmodified natural zeolite.

Elemental analysis of modified zeolite was obtained by X-ray photoelectron spectroscopy (XPS) analysis. As shown in Table 1, XPS analysis results demonstrate that the atomic percentages of Si, C, Ti, and Mn are 30.59%, 39.92%, 19.94%, and 9.54%, respectively. This suggests the zeolite has been coated with nanosized manganese oxide and titanium oxide successfully.

Table 1. XPS analysis of the Mn-Ti Modified zeolite.

Name	Height CPS	FWHM eV	Area (P) CPS.eV	Area (N) TPP-2M	Atomic %
Si2p	3119.57	1.85	6653.8	0.09	30.59
C1s	4037.57	1.68	9192.49	0.12	39.92
Ti2p	8175.82	1.49	28,072.26	0.06	19.94
Mn2p	3694.47	3.67	23,789.49	0.03	9.54

3.1.2. SEM and EDS Analyses of Physical and Chemical Properties

As shown in Figure 4, SEM analysis has the capability to provide an overview of the structure of the natural and the Mn-Ti modified zeolites. The natural zeolite is amorphous, as shown in Figure 4a,b. When it was converted to the Mn-Ti modified zeolite, aggregated spherical shapes covered most of the modified zeolite, as shown in Figure 4c,d. EDS mapping of the modified zeolite is demonstrated in Figure 5, which shows large quantities of Mn, Ti, and O match the formed aggregated spherical shapes. This observation demonstrates a large amount of Mn-Ti is covering the modified zeolite.

3.1.3. FTIR Analysis of Composition

The FTIR spectra of natural and Mn-Ti modified zeolites are shown in Figure 6. Three types of vibration bands are identified, such as the water vibration, the tetrahedron internal vibration, and the vibration between tetrahedrons [16]. For water vibration, OH stretching is observed at 3620 cm^{-1} . Additionally, the bands from 3404 to 3486 cm^{-1} and from 1616 to 1635 cm^{-1} are probably related to H_2O bending mode or bonding between molecules (OH-O) [16,41]. The measurement shows an observable intensity change at $\sim 3620\text{ cm}^{-1}$, $\sim 3400\text{ cm}^{-1}$, and $\sim 1600\text{ cm}^{-1}$ before and after Mn-Ti preparation, which is probably caused by the proton substitution of Mn and Ti. More discussion can be found in the literature [16,41,42]. For the internal vibration, bands at 1037 and 1074 cm^{-1} are likely linked to asymmetric stretching [43]. After the Mn-Ti preparation, the bands are shifted to 1045 and 1094 cm^{-1} . For the vibration between tetrahedrons, a symmetric stretching

band is observed at 792 cm^{-1} [16]. Additionally, bands at 1396 and 918 cm^{-1} are probably corresponding to CO_3 [16,44], which is unobservable after Mn-Ti preparation.

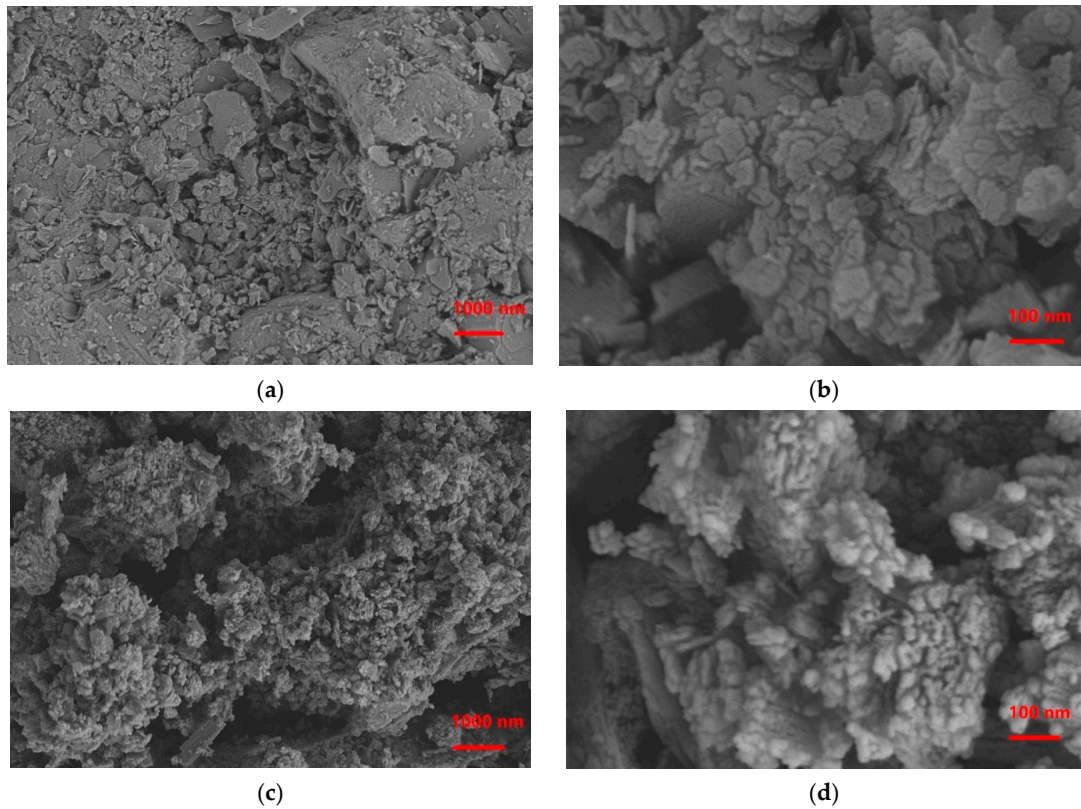


Figure 4. SEM analyses of natural and Mn-Ti modified zeolites: (a,b) are for the natural zeolite, (c,d) are for the Mn-Ti modified zeolite.

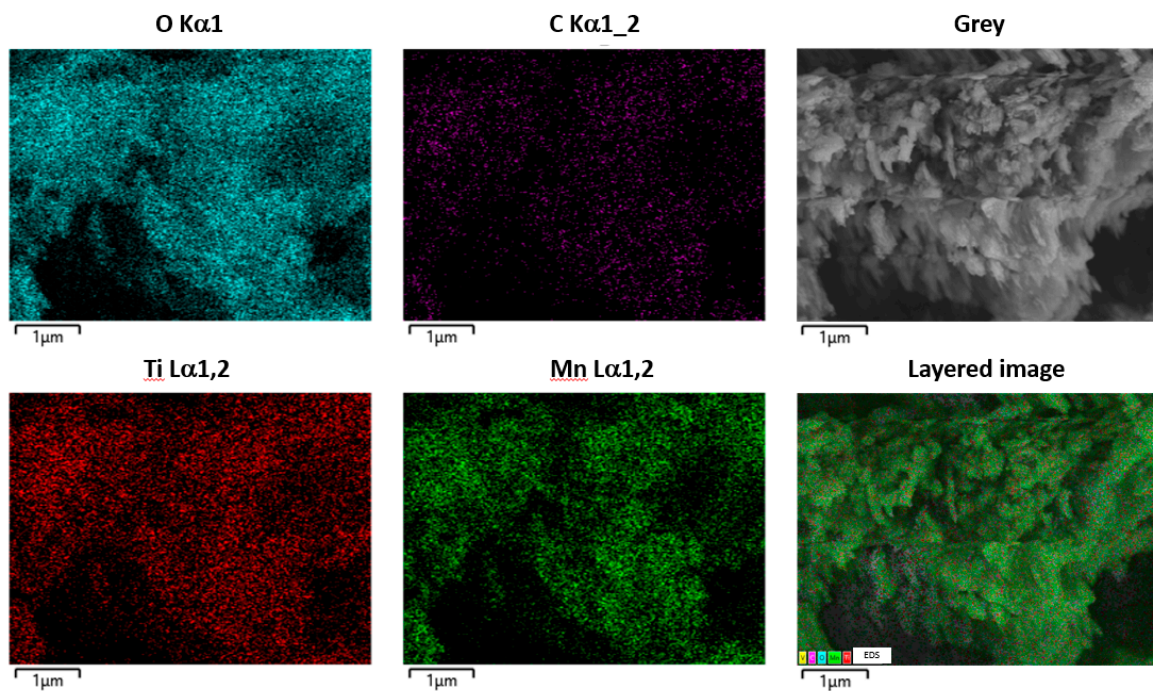


Figure 5. EDS mapping of the Mn-Ti modified zeolite.

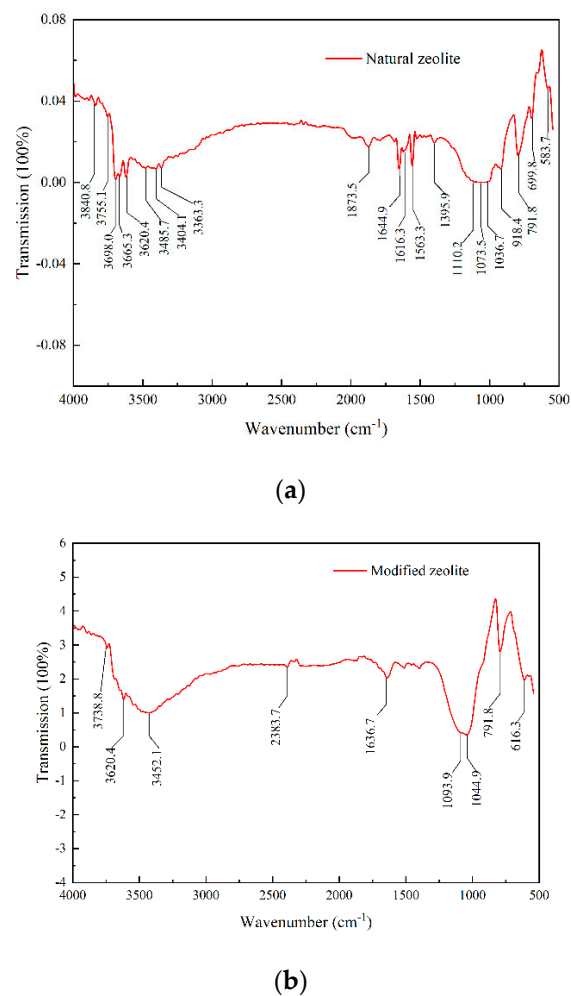


Figure 6. FTIR analyses of zeolites: (a) natural zeolite, (b) modified zeolite.

3.2. Static Adsorption

Static adsorption tests were conducted in a 0.25 L polyethylene conical flask, which was placed in a constant-temperature (25 °C) oscillating water bath. The solution has been stirring at 200 r/min during the experiments. The typical adsorption time is 4-h. In the following, the effects of independent variables are discussed.

3.2.1. Adsorbent Dosage

Varying amounts of the Mn-Ti modified zeolite, 0.1, 0.4, 0.8, 1, 1.5, 2, 2.5, and 3 g, were mixed in a 0.25 L solution with 1×10^{-2} g/L initial fluoride concentration at 25 °C. After a four-hour test time, the remaining fluoride concentration was measured, and the fluoride-removal rate was inferred. Figure 7 demonstrates the fluoride-removal rate change caused by adsorbent dosage. It shows there is a positive correlation between the adsorbent dosage and the fluoride-removal rate. When the adsorbent dosage reached 2 g, the removal rate achieved 77.35%. When the adsorbent dosage was further increased to 3 g, the fluoride-removal capability was not enhanced significantly. This observation shows that increasing the adsorbent dosage can improve the fluoride-removal capability, but the dosage effect will reach a plateau.

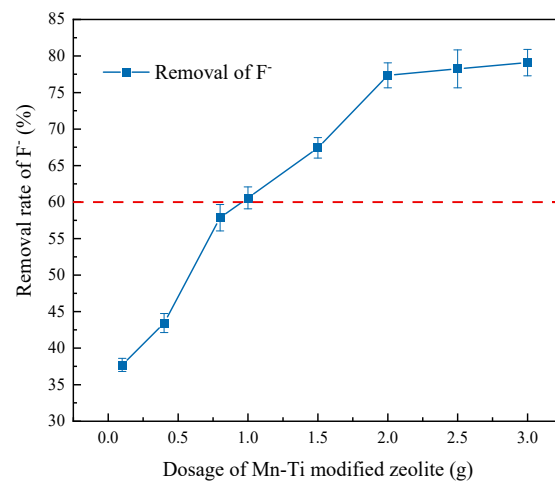


Figure 7. Removal of fluoride ions with different dosage of Mn-Ti modified zeolite. Varying amounts of the Mn–Ti modified zeolite (0.1–3 g) were mixed in a 0.25 L solution with 1×10^{-2} g/L initial fluoride concentration at 25 °C and the test time was 4-h.

3.2.2. PH

PH can alter the adsorption process by chemical effects, including modifying the surface property of adsorbent and adjusting the composition of the wastewater solution. The fluoride-removal capability was tested from pH = 3 to pH = 11. Figure 8 demonstrates the fluoride-removal capability change with pH for the Mn-Ti modified zeolite. At 25 °C, 2 g Mn–Ti modified zeolite was mixed in 0.1 L wastewater solution with a 1×10^{-2} g/L initial fluoride concentration. After 4 h, the remaining fluoride concentration was measured, and fluoride-removal rate was inferred.

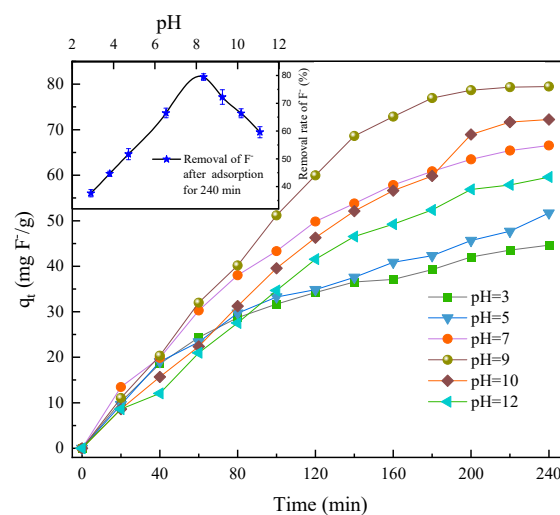


Figure 8. Effect of different pH on removal rate of fluoride ions by the nanosized-manganese oxide/titanium oxide-modified zeolite. The Mn-Ti modified zeolite (2 g) was mixed in a 0.1 L solution with 1×10^{-2} g/L initial fluoride concentration at 25 °C and the test time was 4 h.

Fluoride-removal rate was peaked at pH = 9, and the corresponding maximum removal rate was about 80%. The fluoride-removal rate decreased with the pH at pH > 9. At such conditions, the OH⁻ will be competing with F⁻ in the solution, which occupies the active sites on the Mn-Ti modified zeolite [16,45]. When pH < 7, hydrogen fluoride (HF) is probably dominant in the waste [16,46]. HF is weakly ionized in the solution, which can be the reason of the low fluoride-removal rate.

3.2.3. Adsorption Kinetics

Figure 9 illustrates the adsorption kinetics of fluoride-removal process by the Mn-Ti modified zeolite. Again, 2 g Mn-Ti modified zeolite was mixed with 0.1 L wastewater solution with 1×10^{-2} g/L initial fluoride concentration at 25 °C. Initial pH value was set to 7. Experimental results were used to fit to typical kinetic expressions, such as the Lagergren model [47] and the pseudo-second order [48] model. The fitted expression parameters were determined and are listed in Table 2. The Lagergren model provides a slightly better fitting of the kinetics (Table 2). Traditionally, adsorption kinetic fitting is used to demonstrate the adsorption mechanism based on the fundamental assumptions of each derived equation format. For example, the Lagergren mechanism depicts a solid-capacity reversible adsorption process and is usually applied for physical sorption process of a homogeneous adsorbent, while the pseudo-second order model simulates a chemistry dominant adsorption environment [16]. Therefore, good performance of the Lagergren and the Pseudo-second order models probably illustrate that the current process is a combination of physical sorption and chemisorption.

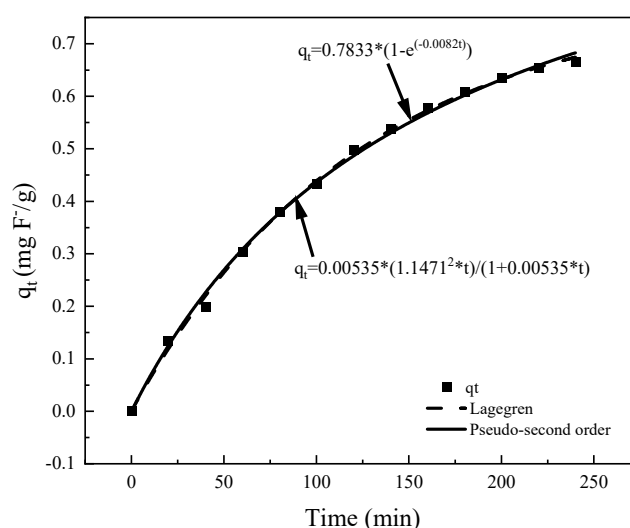


Figure 9. Adsorption kinetic comparison between experiments and models. The Mn–Ti modified zeolite (2 g) was mixed in a 0.1 L solution with 1×10^{-2} g/L initial fluoride concentration at 25 °C and PH = 7 and the test time was 4 h.

Table 2. Fitted parameters of kinetic models.

Lagergren			Pseudo-Second Order		
q_e (mg/g)	KL (1/min)	R^2	q_e (mg/g)	k (g/mg·min)	R^2
0.7833	0.008220	0.9984	1.1467	0.005350	0.9972

The expressions of the models are given in Equations (1) and (2), respectively.

$$\text{Lagergren : } q_t = q_e \left(1 - e^{-K_L t} \right) \quad (1)$$

$$\text{Pseudo - second order : } q_t = \frac{k q_e^2 t}{1 + k q_e t} \quad (2)$$

3.2.4. Adsorption Isotherms

The experimental study of adsorption isotherms was conducted to investigate the effectiveness of the modified zeolite on fluoride-removal. Typical isotherms for fluoride-removal are shown in Figure 10 at different temperatures. Again, 2 g Mn-Ti modified zeolite was

mixed in 0.1 L wastewater containing 1×10^{-2} g/L fluoride. Initial pH value was set to 9. After 4 h, the remaining fluoride concentration was measured. The tested temperature was adjusted from 15 °C to 35 °C. As for the temperature dependence, Figure 10 shows the absorption efficiency is the highest at 25 °C.

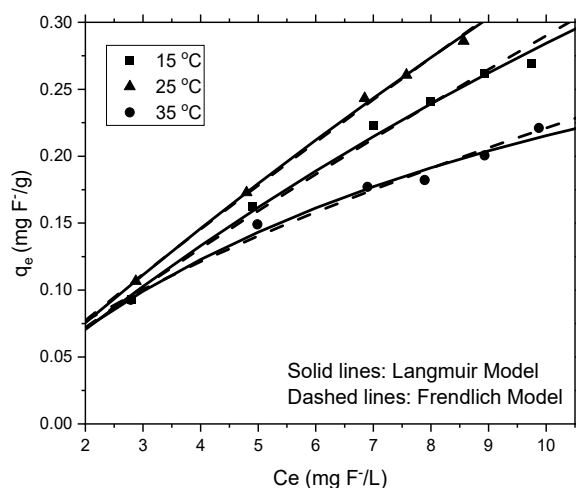


Figure 10. Adsorption isotherms at 15 °C, 25 °C, and 35 °C. The Mn-Ti modified zeolite (2 g) was mixed in a 0.1 L solution with 1×10^{-2} g/L initial fluoride concentration at PH = 9 and the test time was 4-h.

Nonlinear regression fitting was conducted to test the performance of Langmuir and Freundlich isotherm mechanisms. The expressions are given by:

$$\text{Langmuir model : } Q_e = \frac{Q_{\max}K_L C_e}{(1 + K_L C_e)} \tag{3}$$

$$\text{Freundlich model : } Q_e = K_F C_e^{1/n} \tag{4}$$

Table 3 summarizes the fitted model parameters for the two models listed in Equations (3) and (4). Since the Freundlich model is usually applied to illustrate adsorption on inhomogeneous surfaces, we expected a better performance of Freundlich model for the current Mn-Ti modified zeolite. As shown in Table 3, the Freundlich isotherm model shows better performance at different temperatures. Usually speaking, the fitted parameters represent different physical meanings. In the Freundlich model, K_F represents the affinity for the adsorbate and $1/n$ represents the adsorption intensity [49]. On one hand, similar K_F values were observed for different temperatures, which means that affinity is similar at the three temperatures. On the other hand, the highest $1/n$ was observed at 25 °C, which means that the absorption intensity is the highest at 25 °C. The fitted results agree with the direct experimental observations very well.

Table 3. Fitted parameters of adsorption isotherms.

	Langmuir Model			Freundlich Model		
	Q_{\max} (mg/g)	K_L (L/mg)	R^2	K_F (L/mg)	$1/n$	R^2
15 °C	1.1726	0.0320	0.813	0.03956	0.8653	0.989
25 °C	2.1752	0.0180	0.913	0.04114	0.9111	0.998
35 °C	0.4327	0.0995	0.950	0.04890	0.6553	0.981

3.2.5. Competitive Ions

Commonly present ions in wastewater, such as chloride, sulfate, and nitrate, were investigated in this study for their potential influence on fluoride-removal. Again, 2 g Mn-

Ti modified zeolite was mixed in 0.1 L wastewater solution with 1×10^{-2} g/L fluoride at 25 °C. Competitive ions were added into the solution with a concentration at 3×10^{-1} g/L. After 4 h, the residual fluoride concentration was measured. As shown in Figure 11, the fluoride-removal capability is unchanged between the case with chloride and the case with sulfate. On the other hand, the existence of nitrate does have a significant impact on the fluoride-removal compared with the chloride and sulfate. This observation has also been made by Yu et al. [50].

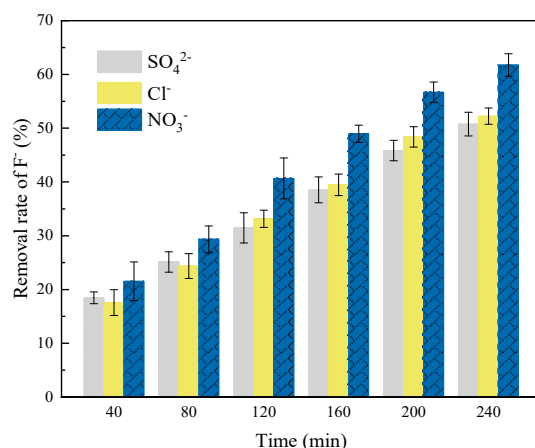


Figure 11. Removal of fluoride ions with different competing ions. The Mn-Ti modified zeolite (2 g) was mixed in a 0.1 L solution with 1×10^{-2} g/L initial fluoride concentration at 25 °C and the test time was 4-h.

3.2.6. Comparison between Natural and Mn-Ti Modified Zeolites

A comparison between the natural zeolite and the Mn-Ti modified zeolite is shown in Figure 12. In this comparison, 2 g zeolites were placed in the 0.25 L wastewater solution with 1×10^{-2} g/L initial fluoride at 25 °C. The fluoride concentration was measured every 20 min to monitor the fluoride time history. In the static system, the modified zeolite shows a much stronger adsorption capability than the natural zeolite. Figure 12 shows that the Mn-Ti modified zeolite provides not only a faster adsorption speed, but also a lower equilibrium fluoride concentration.

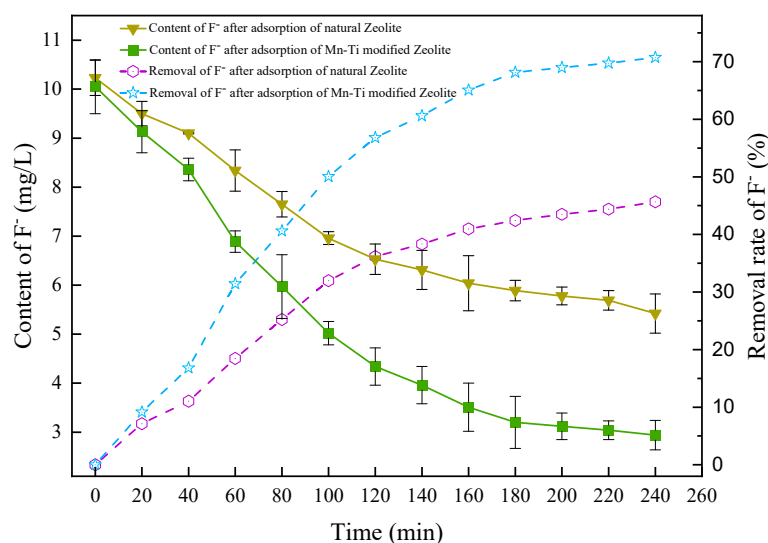


Figure 12. Removal of fluoride ions with natural and Mn-Ti modified zeolites; 2 g of zeolites were placed in the 0.25 L wastewater solution with 1×10^{-2} g/L initial fluoride at 25 °C.

3.2.7. Comparison with Studies in the Literature

To provide a direct comparison of the Mn-Ti modified zeolite with the studies in the literature, a literature review is conducted. The results are shown in Table 4. The experimental conditions, such as PH, test time, operating temperature, and initial fluoride concentration are listed. Moreover, the maximum adsorption capacities of the adsorbents were compared. Notably, the major objective of the current study was to provide a direction comparison between the natural zeolite and the Mn-Ti modified zeolite. The comparison with studies in the literature may be misleading since the material preparation procedures can be very different.

Table 4. A comparison of the adsorption capacity.

Adsorbents	Experimental Conditions				q_e (mg/g)
	pH	Time (h)	Temperature (°C)	Initial F^- Concentration (mg/L)	
Zeolite-Zr [51]	7	24	30	2.5	4.427
Zeolite-La [51]	7	24	30	2.5	1.691
Zeolite-Al [51]	7	24	30	2.5	1.71
Boehmite [52]	6.8	24	25	10	2.057
Synthetic hydroxyapatite [53]	2	2	25	5	0.489
Fe^{3+} activated quartz [54]	6	1.6	20	3×10^{-5}	1.16
Mn-Ti modified zeolite	7	4	25	10	2.175

3.3. Dynamic Adsorption

To study the adsorption capability of the Mn-Ti modified zeolite in practical systems, an adsorption column with continued flow was designed to test its adsorption in a dynamic system. Dynamic adsorption tests were conducted in an adsorption column made with plexiglass: the diameter of the column was 20 mm and the length was 1500 mm. Zeolite powders could be filled in the column and the wastewater containing fluoride flow through the column in a steady speed. Sampling points were carefully designed to make sure the samplings could be obtained at different locations and times.

3.3.1. Adsorbent Thickness

The effect of adsorbent thickness was tested with adsorbent columns filling with modified zeolite at different thicknesses. In the current study, the tested thicknesses were 40, 60, and 80 cm. The initial F^- concentration was set to 1×10^{-2} g/L, PH was set to 7, and flow speed was set to 4 mL/min. About 5 mL sampling water was collected for every 30 min. The results were analyzed and are shown in Figure 13.

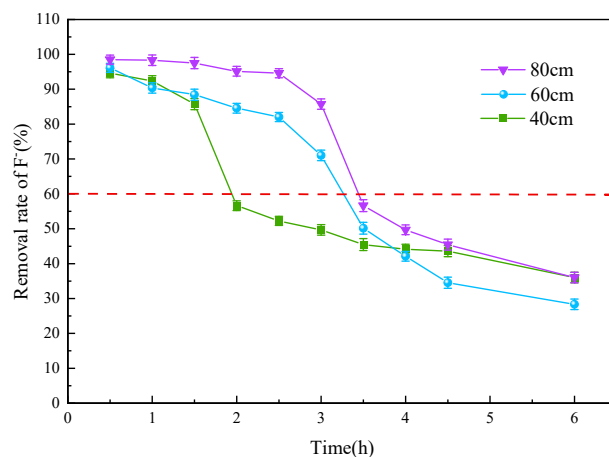


Figure 13. Effect of adsorbent thickness in an adsorbent column. The initial F^- concentration was set to 1×10^{-2} g/L, PH was set to 7, and flow speed was set to 4 mL/min.

Figure 13 shows that adjusting the adsorbent thickness has an observable effect on the removal rate of F^- . The case with 80 cm adsorbent thickness presents the highest removal rate, and it also shows the effectiveness of the adsorbent lasts for a longer time. At about 3 h, there is a sharp drop of the removal rate, which means the adsorbent effectiveness is decreasing. If we define the effectiveness period as the period between the start of the experiment and the time when the removal rate of F^- is lower than 60%, the effectiveness periods of the cases with 40, 60, and 80 cm adsorbent thicknesses are about 2, 3, and 3.5 h, respectively. The effectiveness period shows a strong linear correlation with the adsorbent thickness.

3.3.2. Flow Velocity

Flow velocity is an important parameter in a dynamic system. Therefore, the effect of flow speed was investigated here. The initial F^- concentration was set to 1×10^{-2} g/L, pH was set to 7. The flow speed was adjusted from 4 mL/min to 8 mL/min to test the effect of the flow speed. About 5 mL sampling water were collected every 30 min. The fluoride concentration was monitored, and the results are shown in Figure 14.

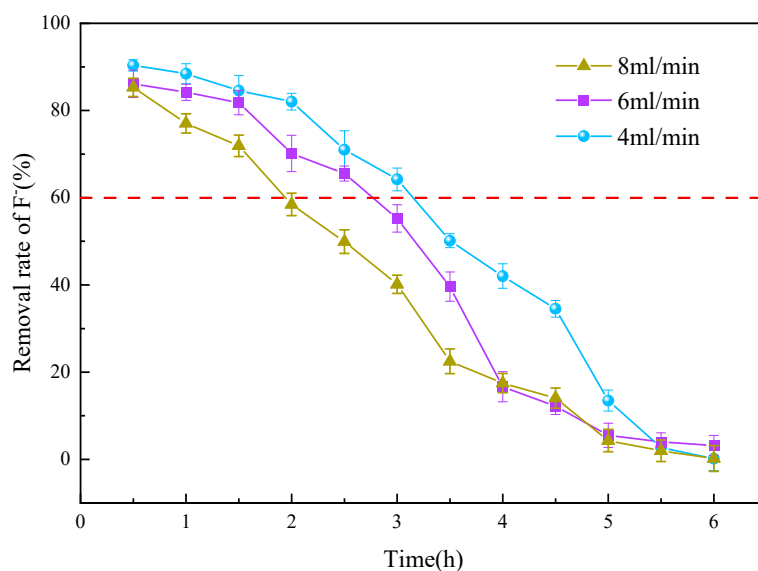


Figure 14. Effect of flow speed in an adsorbent column. The initial F^- concentration was set to 1×10^{-2} g/L, and pH was set to 7.

Figure 14 shows that the removal rate can be affected by flow speed significantly. At each time step, the adsorbent performance is much better with low flow speed. For example, the removal rates of the 4, 6, and 8 mL/min cases are about 82%, 70%, and 60% at 2 h, respectively. Therefore, for a better adsorbent performance, low flow speed is recommended. Additionally, the effectiveness periods for the 4, 6, and 8 mL/min cases are about 3.5, 2.6, and 2 h, respectively. The effectiveness period of the case with 8 mL/min flow speed is much shorter than the other two cases. We further define the effectiveness volume as the time of effectiveness period and the flow speed, which shows the overall volume of wastewater going through the adsorbent column in the effectiveness period. The effectiveness volumes of the 4, 6, and 8 mL/min cases are 840, 936, and 960 mL, respectively. The relatively consistent effectiveness volumes demonstrate that the total volume of the wastewater that can be processed by a certain amount of modified zeolite is independent of the flow speed.

3.3.3. Initial Fluoride Concentration

The effect of initial fluoride concentration was also studied. The initial fluoride concentration was adjusted from 3×10^{-3} g/L to 1×10^{-2} g/L. pH was set to 7. The

flow speed was set to 4 mL/min. About 5 mL sampling water was collected for every 30 min. The fluoride concentration was monitored, and the measured results are depicted in Figure 15.

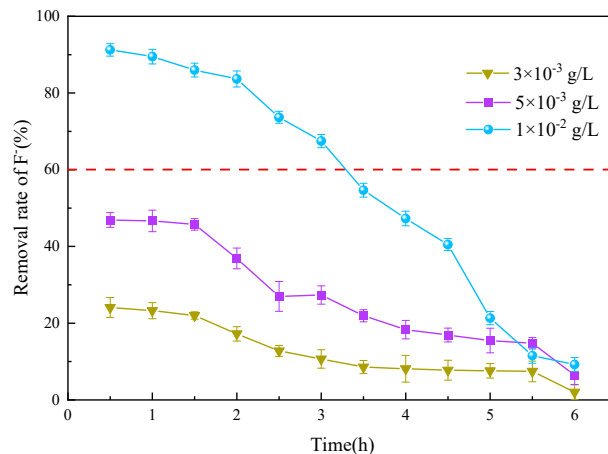


Figure 15. Effect of initial F^- concentration in an adsorbent column. The pH was set to 7. The flow speed was set to 4 mL/min.

Figure 15 shows the effectiveness of the adsorbent is highly dependent on the initial fluoride concentration. When the initial concentration is 1×10^{-2} g/L, the adsorbent is efficient enough to remove 90% fluoride of the wastewater at least at early times. When the initial concentration is 3×10^{-3} g/L, only about 25% fluoride can be removed. This is beneficial to the practical systems since the typical target of wastewater processing is to reduce fluoride concentration to a certain level instead of removing all the fluoride. The suppressed performance with low fluoride concentration wastewater may be beneficial to help the modified zeolite achieve a longer effectiveness period in practical systems.

3.3.4. pH

The pH effect was studied again in the dynamic system similar with the static adsorption section. The initial fluoride concentration was set to 1×10^{-2} g/L. Flow speed was set to 4 mL/min. pH was adjusted from 4 to 9. About 5 mL sampling water were collected every 30 min. The fluoride concentration was measured, and the fluoride-removal rates are illustrated in Figure 16.

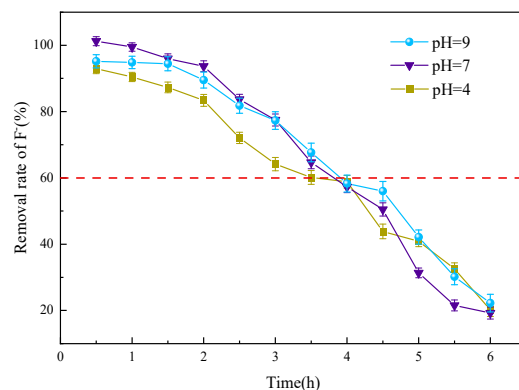


Figure 16. Effect of pH in an adsorbent column. The initial fluoride concentration was set to 1×10^{-2} g/L. Flow speed was set to 4 mL/min.

The pH effect in the dynamic system is less significant than the similar test in static system conducted in Section 3.2. The case with pH = 9 performs in a way similar to the case

with pH = 7 during the six-hour test time. The case with pH = 4 has a much lower removal rate, which probably comes from the weakly ionized HF formation.

3.3.5. Comparison between Natural and Mn-Ti Modified Zeolites

To compare the natural zeolite and the Mn-Ti modified zeolite in an operating condition close to real applications, the dynamic adsorbent tests were conducted in adsorbent columns filling with different zeolites. The initial fluoride concentration was set to 1×10^{-2} g/L. Flow speed was set to 4 mL/min. Additionally, the adsorbent thickness was set to 60 cm. About 5 mL sampling water were collected every 30 min. The fluoride concentration was measured, and the results are shown in Figure 17.

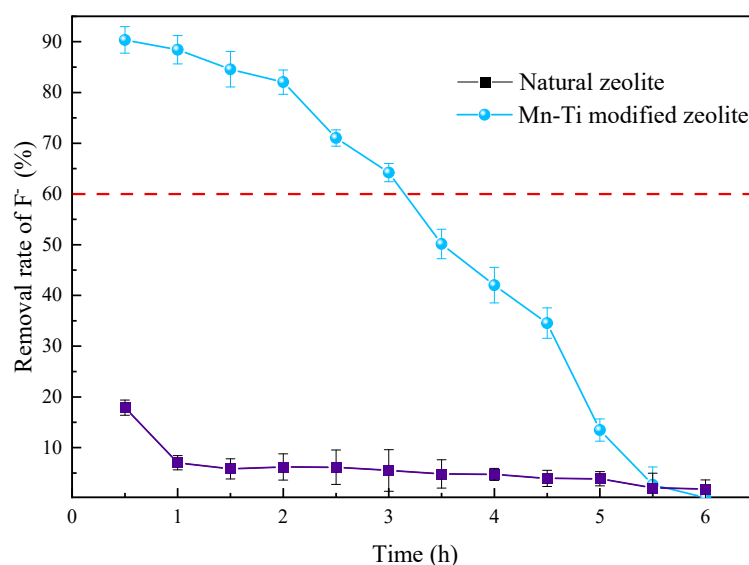


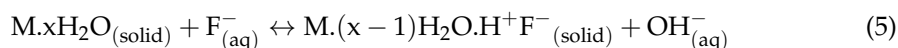
Figure 17. Comparison of adsorbent capabilities of zeolite and modified zeolite in an adsorbent column. The initial fluoride concentration was set to 1×10^{-2} g/L. Flow speed was set to 4 mL/min.

Figure 17 demonstrates that the Mn-Ti modified zeolite provides a much higher fluoride-removal rate than the natural zeolite, which suggests the necessity to modify the natural zeolite with nano materials.

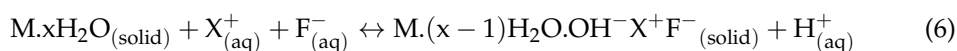
3.4. Adsorption Mechanism

It is well known that the fluoride-removal mechanism of modified zeolites is complicated, involving both physical and chemisorption [55]. Metal oxide adsorption mechanisms have been extensively discussed by many researchers [56–58]. To better understand the chemisorption process of the Mn-Ti modified zeolite, the most probable mechanisms for fluoride adsorption on metal oxide surface can be illustrated as [59]:

In acidic environment:



In basic environment:



where M represents metal oxides and X^+ is the cationic species.

The fluoride-removal mechanism on a metal oxide surface was noticed as a complicated phenomenon. Tor [60] and Sarkar et al. [61] had a detailed discussion about the fluoride-removal process for metal oxides. In those pioneer works, they indicated that

the exchange between absorbent surface groups and fluoride ions happens since both fluoride ions and hydroxyl ions have a comparable ionic radius from their isoelectronic nature.

In the current study, the reasons of the improved adsorption capability of the Mn-Ti modified zeolite can be summarized in the following. On one hand, the fluoride ions will be attracted by metal cations under Coulomb force when the fluoride ions get close to the metal oxides on the surface of the modified zeolite. At same time, the fluoride ions will combine with the protonated hydroxyl group to form a hydrated metal fluoride precipitate. On the other hand, the above process can be achieved by directly capturing hydrogen ions using the Mn-Ti active metal oxide groups on the surface of the modified zeolite to generate hydrated metal fluoride precipitation. Additionally, the cation groups on the surface of the modified zeolite can also directly use electrostatic attraction to adsorb fluoride ions using the multi-scale micropores or replace fluoride ions with hydroxyl groups on the surface of the modified zeolite to remove them from the water.

4. Conclusions

The fluoride-removal capability of Mn-Ti modified zeolite is studied in the current work. Physical and chemical properties of the natural and Mn-Ti modified zeolites were characterized by SEM and EDS. XRD and FTIR were used to analyze the surface change before and after the adsorption. A static system was first used to characterize the fluoride-removal efficiency of the Mn-Ti Modified zeolite in a static. The Mn-Ti modified zeolite showed a much stronger fluoride-removal capability than the natural zeolite. The effects of independent variables, such as adsorbent dosage, pH, and competitive ions, were studied. There are several important findings: (1) there is a positive correlation between the adsorbent dosage and the fluoride-removal rate; (2) fluoride-removal rate is peaked at pH = 9, and the corresponding maximum removal rate is about 80%; (3) The tested temperature is adjusted from 15 °C to 35 °C. The absorption efficiency is the highest at 25 °C; (4) the fluoride-removal capability is unchanged between the case with chloride and the case with sulfate. On the other hand, the existence of nitrate does have a significant impact on the fluoride-removal compared with the chloride and sulfate; (5) Adsorption kinetics analyses show that the adsorption process is a combination of the physical sorption and chemisorption. To study the Mn-Ti modified zeolite in an operating condition close to practical systems, an adsorption column was designed to study the fluoride-removal capability of Mn-Ti modified zeolite in a dynamic system. Again, a much stronger adsorption capability was observed for the Mn-Ti modified zeolite. The effects of independent variables, such as adsorbent thickness, flow velocity, initial fluoride concentration, and pH were studied. There are also several important findings: (1) adjusting the adsorbent thickness has an observable effect on the removal rate of F^- . The case with a higher adsorbent thickness presents a higher removal rate; (2) for a better adsorbent performance, low flow speed is recommended; (3) The effectiveness of the adsorbent is suppressed at low fluoride concentrations; (4) the case with pH = 9 performs in a way similar to the case with pH = 7 in the dynamic system. Additionally, the adsorption mechanism of the Mn-Ti modified zeolite is also discussed. The reasons of the improved adsorption capability of the Mn-Ti modified zeolite are summarized as: hydrated metal fluoride precipitate formation and electrostatic attraction of cation groups.

Author Contributions: Conceptualization, C.Z. and B.Y.; methodology, B.Y. and B.Q.; software, G.S.; validation, B.Y., B.Q., J.T. and Y.T.; formal analysis, G.S. and C.J.; investigation, B.Y.; resources, C.Z.; data curation, W.W., X.W. and M.Z.; writing—original draft preparation, B.Y.; writing—review and editing, B.Y. and B.Q.; visualization, C.Z.; supervision, B.X.; project administration, B.X.; funding acquisition, C.Z. All authors have read and agreed to the published version of the manuscript.

Funding: This research was funded by the financial support provided by the National Key R&D Program of China (No. 2018YFC0406403) and the Special Fund for Fundamental Scientific Research Business Expenses of Central Universities (China, No. 2011QH01).

Institutional Review Board Statement: Not applicable.

Informed Consent Statement: Not applicable.

Data Availability Statement: Not applicable.

Acknowledgments: We gratefully acknowledge the financial support provided by the National Key R&D Program of China (No.2018YFC0406403) and the Special Fund for Fundamental Scientific Research Business Expenses of Central Universities (China, NO.2011QH01).

Conflicts of Interest: The authors declare no conflict of interest.

References

1. Edition, F. Guidelines for drinking water quality. *WHO Chron.* **2011**, *38*, 104–108.
2. Handa, B.K. Geochemistry and genesis of fluoride-containing ground waters in India. *Ground Water* **1975**, *13*, 275–281. [[CrossRef](#)]
3. Fuhong, R.; Shuqin, J. Distribution and formation of high-fluorine groundwater in China. *Environ. Earth Sci.* **1988**, *12*, 3–10. [[CrossRef](#)]
4. Malago, J.; Makoba, E.; Muzuka, A.N.N. fluoride levels in surface and groundwater in Africa: A review. *Am. J. Water Sci. Eng.* **2017**, *3*, 1. [[CrossRef](#)]
5. Armienta, M.A.; Segovia, N. Arsenic and fluoride in the groundwater of Mexico. *Environ. Geochem. Health* **2008**, *30*, 345–353. [[CrossRef](#)] [[PubMed](#)]
6. Drondina, R.; Romanov, A.; Matveevich, V.; Motspan, V.; Shafranskij, V. Electrochemical method to remove fluorine from waters. The study of its mechanism. *J. Fluor. Chem.* **1989**, *45*, 58. [[CrossRef](#)]
7. Singh, R.K.; Multari, N.; Nau-Hix, C.; Woodard, S.; Nickelsen, M.; Thagard, S.M.; Holsen, T.M. Removal of poly- and per-fluorinated compounds from ion exchange regenerant still bottom samples in a plasma reactor. *Environ. Sci. Technol.* **2020**, *54*, 13973–13980. [[CrossRef](#)]
8. Turner, B.D.; Binning, P.; Stipp, S.L.S. Fluoride removal by calcite: Evidence for fluorite precipitation and surface adsorption. *Environ. Sci. Technol.* **2005**, *39*, 9561–9568. [[CrossRef](#)] [[PubMed](#)]
9. Amor, Z.; Bariou, B.; Mameri, N.; Taky, M.; Nicolas, S.; Elmidaoui, A. Fluoride removal from brackish water by electro dialysis. *Desalination* **2001**, *133*, 215–223. [[CrossRef](#)]
10. Zeni, M.; Riveros, R.; Melo, K.; Primieri, R.; Lorenzini, S. Study on fluoride reduction in artesian well—water from electro dialysis process. *Desalination* **2005**, *185*, 241–244. [[CrossRef](#)]
11. Keri, R.S.; Hosamani, K.M.; Reddy, H.R.S.; Nataraj, S.K.; Aminabhavi, T. Application of the electro dialytic pilot plant for fluoride removal. *J. Water Chem. Technol.* **2011**, *33*, 293–300. [[CrossRef](#)]
12. Sehn, P. Fluoride removal with extra low energy reverse osmosis membranes: Three years of large scale field experience in Finland. *Desalination* **2008**, *223*, 73–84. [[CrossRef](#)]
13. Schneider, R.; Middlebrooks, E. Arsenic and fluoride removal from groundwater by reverse osmosis. *Environ. Int.* **1983**, *9*, 289–291. [[CrossRef](#)]
14. Min, B.R.; Gill, A.L.; Gill, W.N. A note on fluoride removal by reverse osmosis. *Desalination* **1984**, *49*, 89–93. [[CrossRef](#)]
15. Shen, J.; Schäfer, A. Removal of fluoride and uranium by nanofiltration and reverse osmosis: A review. *Chemosphere* **2014**, *117*, 679–691. [[CrossRef](#)]
16. Velazquez-Peña, G.C.; Olguín-Gutiérrez, M.T.; Solache-Ríos, M.J.; Fall, C. Significance of FeZr-modified natural zeolite networks on fluoride removal. *J. Fluor. Chem.* **2017**, *202*, 41–53. [[CrossRef](#)]
17. Tabi, R.N.; Agyemang, F.O.; Mensah-Darkwa, K.; Arthur, E.K.; Gikunoo, E.; Momade, F. Zeolite synthesis and its application in water defluorination. *Mater. Chem. Phys.* **2021**, *261*, 124229. [[CrossRef](#)]
18. Gao, Y.; Li, M.; Ru, Y.; Fu, J. Fluoride removal from water by using micron zirconia/zeolite molecular sieve: Characterization and mechanism. *Groundw. Sustain. Dev.* **2021**, *13*, 100567. [[CrossRef](#)]
19. Vinati, A.; Mahanty, B.; Behera, S. Clay and clay minerals for fluoride removal from water: A state-of-the-art review. *Appl. Clay Sci.* **2015**, *114*, 340–348. [[CrossRef](#)]
20. Karthikeyan, G.; Pius, A.; Alagumuthu, G. Fluoride adsorption studies of montmorillonite clay. *Indian J. Chem. Technol.* **2005**, *12*, 263–272.
21. Nabbou, N.; Belhachemi, M.; Boumelik, M.; Merzougui, T.; Lahcene, D.; Harek, Y.; Zorpas, A.A.; Jeguirim, M. Removal of fluoride from groundwater using natural clay (kaolinite): Optimization of adsorption conditions. *C. R. Chim.* **2019**, *22*, 105–112. [[CrossRef](#)]
22. Liang, S.; Xue, Y.; Gao, B.; Yang, K. Removal of fluoride from aqueous solution by TiO₂-based composites. *J. Taiwan Inst. Chem. Eng.* **2017**, *74*, 205–210. [[CrossRef](#)]
23. Fukahori, S.; Ito, M.; Fujiwara, T. Removal mechanism of sulfamethazine and its intermediates from water by a rotating advanced oxidation contactor equipped with TiO₂-high-silica zeolite composite sheets. *Environ. Sci. Pollut. Res.* **2018**, *25*, 29017–29025. [[CrossRef](#)]
24. Liu, S.; Lim, M.; Amal, R. TiO₂-coated natural zeolite: Rapid humic acid adsorption and effective photocatalytic regeneration. *Chem. Eng. Sci.* **2014**, *105*, 46–52. [[CrossRef](#)]
25. Con, T.H.; Thao, P.; Dai, T.X.; Loan, D.K. Application of nano dimensional MnO₂ for high effective sorption of arsenic and fluoride in drinking water. *Environ. Sci.* **2013**, *1*, 69–77. [[CrossRef](#)]

26. Mudzielwana, R.; Gitari, M.W. Removal of fluoride from groundwater using MnO₂ bentonite-smectite rich clay soils composite. *Groundw. Sustain. Dev.* **2021**, *14*, 100623. [[CrossRef](#)]
27. Mudzielwana, R.; Gitari, M.W.; Akinyemi, S.A.; Msagati, T.A.M. Synthesis and physicochemical characterization of MnO₂ coated Na-bentonite for groundwater defluoridation: Adsorption modelling and mechanistic aspect. *Appl. Surf. Sci.* **2017**, *422*, 745–753. [[CrossRef](#)]
28. Bahiraei, A.; Behin, J. Sonochemical immobilization of MnO₂ nanoparticles on NaP-zeolite for enhanced Hg (II) adsorption from water. *J. Environ. Chem. Eng.* **2020**, *8*, 103790. [[CrossRef](#)]
29. Zeng, Y.; Xue, Y.; Liang, S.; Zhang, J. Removal of fluoride from aqueous solution by TiO₂ and TiO₂-SiO₂ nanocomposite. *Chem. Speciat. Bioavailab.* **2016**, *29*, 25–32. [[CrossRef](#)]
30. O'Neill, M.A.; Cozens, F.L.; Schepp, N.P. Photogeneration and migration of electrons and holes in zeolite NaY. *J. Phys. Chem. B* **2001**, *105*, 12746–12758. [[CrossRef](#)]
31. Liu, C.; Zhang, R.; Wei, S.; Wang, J.; Liu, Y.; Li, M.; Liu, R. Selective removal of H₂S from biogas using a regenerable hybrid TiO₂/zeolite composite. *Fuel* **2015**, *157*, 183–190. [[CrossRef](#)]
32. Hashimoto, K.; Wasada, K.; Osaki, M.; Shono, E.; Adachi, K.; Toukai, N.; Kominami, H.; Kera, Y. Photocatalytic oxidation of nitrogen oxide over titania-zeolite composite catalyst to remove nitrogen oxides in the atmosphere. *Appl. Catal. B Environ.* **2001**, *30*, 429–436. [[CrossRef](#)]
33. Camacho, L.M.; Parra, R.R.; Deng, S. Arsenic removal from groundwater by MnO₂-modified natural clinoptilolite zeolite: Effects of pH and initial feed concentration. *J. Hazard. Mater.* **2011**, *189*, 286–293. [[CrossRef](#)]
34. Zou, W.; Han, R.; Chen, Z.; Shi, J.; Liu. Characterization and properties of manganese oxide coated zeolite as adsorbent for removal of copper(II) and lead(II) ions from solution. *J. Chem. Eng. Data* **2006**, *51*, 534–541. [[CrossRef](#)]
35. Han, R.; Zou, W.; Li, H.; Li, Y.; Shi, J. Copper(II) and lead(II) removal from aqueous solution in fixed-bed columns by manganese oxide coated zeolite. *J. Hazard. Mater.* **2006**, *137*, 934–942. [[CrossRef](#)]
36. Lyu, C.; Yang, X.; Zhang, S.; Zhang, Q.; Su, X. Preparation and performance of manganese-oxide-coated zeolite for the removal of manganese-contamination in groundwater. *Environ. Technol.* **2019**, *40*, 878–887. [[CrossRef](#)]
37. Zhu, B.L.; Lv, L.; Wang, X.J. Preparation and magnetic properties of α -MnO₂ nanoparticles. In *Key Engineering Materials*; Trans Tech Publications Ltd.: Zürich, Switzerland, 2012; Volume 492, pp. 264–267.
38. Huang, X.; Lv, D.; Yue, H.; Attia, A.; Yang, Y. Controllable synthesis of α - and β -MnO₂: Cationic effect on hydrothermal crystallization. *Nanotechnology* **2008**, *19*, 225606. [[CrossRef](#)]
39. Hashemzadeh, F.; Kashani-Motlagh, M. Hydrothermal synthesis and characterisation of MnO₂ nanostructures. *Int. J. Nanomanuf.* **2010**, *5*, 260–267. [[CrossRef](#)]
40. Fischer, K. The crystal structure determination of the zeolite gismondite. CaAl₂Si₂O₈ · 4H₂O. *Am. Mineral. J. Earth Planet. Mater.* **1963**, *48*, 664–672.
41. Akgül, M. Enhancement of the anionic dye adsorption capacity of clinoptilolite by Fe³⁺-grafting. *J. Hazard. Mater.* **2014**, *267*, 1–8. [[CrossRef](#)] [[PubMed](#)]
42. Góra-Marek, K.; Brylewska, K.; Tarach, K.A.; Rutkowska, M.; Jabłońska, M.; Choi, M.; Chmielarz, L. IR studies of Fe modified ZSM-5 zeolites of diverse mesopore topologies in the terms of their catalytic performance in NH₃-SCR and NH₃-SCO processes. *Appl. Catal. B Environ.* **2015**, *179*, 589–598. [[CrossRef](#)]
43. Breck, D.W.; Breck, D.W. *Zeolite Molecular Sieves: Structure, Chemistry, and Use*; John Wiley & Sons: Hoboken, NJ, USA, 1973.
44. Gunasekaran, S.; Anbalagan, G.; Pandi, S. Raman and infrared spectra of carbonates of calcite structure. *J. Raman Spectrosc.* **2006**, *37*, 892–899. [[CrossRef](#)]
45. Asgari, G.; Roshani, B.; Ghanizadeh, G. The investigation of kinetic and isotherm of fluoride adsorption onto functionalize pumice stone. *J. Hazard. Mater.* **2012**, *217–218*, 123–132. [[CrossRef](#)] [[PubMed](#)]
46. Bia, G.; De Pauli, C.P.; Borgnino, L. The role of Fe(III) modified montmorillonite on fluoride mobility: Adsorption experiments and competition with phosphate. *J. Environ. Manag.* **2012**, *100*, 1–9. [[CrossRef](#)] [[PubMed](#)]
47. Aksakal, O.; Uzun, H. Equilibrium, kinetic and thermodynamic studies of the biosorption of textile dye (Reactive Red 195) onto *Pinus sylvestris* L. *J. Hazard. Mater.* **2010**, *181*, 666–672. [[CrossRef](#)] [[PubMed](#)]
48. Lin, J.; Wang, L. Comparison between linear and non-linear forms of pseudo-first-order and pseudo-second-order adsorption kinetic models for the removal of methylene blue by activated carbon. *Front. Environ. Sci. Eng. China* **2009**, *3*, 320–324. [[CrossRef](#)]
49. Hamdaoui, O.; Naffrechoux, E. Modeling of adsorption isotherms of phenol and chlorophenols onto granular activated carbon: Part I. Two-parameter models and equations allowing determination of thermodynamic parameters. *J. Hazard. Mater.* **2007**, *147*, 381–394. [[CrossRef](#)]
50. Yu, Y.; Yu, L.; Chen, J.P. Adsorption of fluoride by Fe–Mg–La triple-metal composite: Adsorbent preparation, illustration of performance and study of mechanisms. *Chem. Eng. J.* **2015**, *262*, 839–846. [[CrossRef](#)]
51. Samatya, S.; Yüksel, Ü.; Yüksel, M.; Kabay, N. Removal of fluoride from water by metal ions (Al³⁺, La³⁺ and ZrO₂⁺) loaded natural zeolite. *Sep. Sci. Technol.* **2007**, *42*, 2033–2047. [[CrossRef](#)]
52. Becerril, J.J.; Solache-Ríos, M.; García-Sosa, I. Fluoride removal from aqueous solutions by boehmite. *Water Air Soil Pollut.* **2011**, *223*, 1073–1078. [[CrossRef](#)]
53. Gao, S.; Sun, R.; Wei, Z.; Zhao, H.; Li, H.; Hu, F. Size-dependent defluoridation properties of synthetic hydroxyapatite. *J. Fluor. Chem.* **2009**, *130*, 550–556. [[CrossRef](#)]

54. Fan, X.; Parker, D.J.; Smith, M.D. Adsorption kinetics of fluoride on low cost materials. *Water Res.* **2003**, *37*, 4929–4937. [[CrossRef](#)]
55. Sujana, M.; Anand, S. Ferric hydroxide: Preparation, characterisation and fluoride removal studies from water. *Desalin. Water Treat.* **2013**, *52*, 6453–6463. [[CrossRef](#)]
56. Ma, Z.; Zhang, Q.; Weng, X.; Mang, C.; Si, L.; Guan, Z.; Cheng, L. Fluoride ion adsorption from wastewater using magnesium(II), aluminum(III) and titanium(IV) modified natural zeolite: Kinetics, thermodynamics, and mechanistic aspects of adsorption. *J. Water Reuse Desalin.* **2017**, *8*, 479–489. [[CrossRef](#)]
57. Raichur, A.; Basu, M.J. Adsorption of fluoride onto mixed rare earth oxides. *Sep. Purif. Technol.* **2001**, *24*, 121–127. [[CrossRef](#)]
58. Ruthven, D.M. *Principles of Adsorption and Adsorption Processes*; John Wiley & Sons: Hoboken, NJ, USA, 1984.
59. Balistreri, L.S.; Murray, J.W. The surface chemistry of goethite (alpha FeOOH) in major ion seawater. *Am. J. Sci.* **1981**, *281*, 788–806. [[CrossRef](#)]
60. Tor, A. Removal of fluoride from an aqueous solution by using montmorillonite. *Desalination* **2006**, *201*, 267–276. [[CrossRef](#)]
61. Sarkar, M.; Banerjee, A.; Pramanick, P.P. Kinetics and mechanism of fluoride removal using laterite. *Ind. Eng. Chem. Res.* **2006**, *45*, 5920–5927. [[CrossRef](#)]